ARMA 13-347

Laboratory-scale strain and temperature response of a distributed optical fiber sensor

Madjdabadi, B. M.
Civil Engineering Department, University of Waterloo, Waterloo, Ontario, Canada

Benoît Valley
Geological Institute, ETH Zürich, Switzerland

Leah Siczkar
Civil Engineering Department, University of Waterloo, Waterloo, Ontario, Canada

Maurice B. Dusseault
Earth and Environmental Sciences Department, University of Waterloo, Waterloo, Ontario, Canada

Peter K. Kaiser
CEMI, Sudbury, Ontario, Canada

This paper was prepared for presentation at the 46th US Rock Mechanics / Geomechanics Symposium held in Chicago, IL, USA, 24-27 June 2012.

ABSTRACT: Distributed optical fiber sensors (DOFSs), used initially in structural health monitoring for high-rise buildings and bridges, are attracting attention in the field of underground structures, including mining. Designed for long-term study of deformations, DOFSs are more efficient when installed away from excavation damaged zone (EDZ) in a borehole filled with a grout mixture to measure elastic strain field responses to excavations. The DOFS sensing cable, as a component of a complex compliance system, i.e. rockmass and grout, is being assessed through laboratory work.

A test program is underway to observe DOFS response to various perturbations including strain and joint displacement. Initially, tests on unstrained sensors are performed in order to assess measurement repeatability and noise-to-signal ratio at both local and global scales. Then, the various lengths of the cable, from 1 m down to 1 cm, will be stretched up to 0.5% strain. In other tests, the same lengths of the cable will be exposed to shear displacement, such as might occur in the vicinity of a joint or fault that experiences shear.

The results from these tests will answer uncertainties and questions regarding the scaling factor between straining sections over a full sampling window, i.e. spatial resolution, and a partial sampling window, i.e. validity of calibration factors provided by the supplier, and assessing effects of coating and plastic protective layers of the sensor. Issues such as shear deformation responses of cable and bending direction of the cable are being evaluated.

Initial results on unstrained cable to assess measurement repeatability showed variability in length assessment between successive readings. This variability particularly impacts the data interpretation from the strain sensors since these sensors present locally large Brillouin frequency gradients which results in locally large variability in differential readings. Our detailed experimental results will be presented in the paper.

Keywords: DOFS, Smart Profile, DiTeSt, Spatial resolution, Brillouin frequency, strain

1. INTRODUCTION

Newly developed distributed optical fiber sensors (DOFSs) have promising application in engineering contexts especially when the size of the structure to monitor is large. These sensors have been used for monitoring of landslide activity [1], integrity of embankments and dams [2], bridges [3], and pipelines in the oil sector [4, 5]. They have also been applied to the monitoring of underground excavations including shallow tunnels [6] and deep mines [7, 8]. Since natural materials such as soils and

rocks contain many heterogeneities across all scales as well as time dependent behavior, the opportunity presented by these new distributed sensing technologies is particularly attractive.

These sensors have also been tested in laboratory conditions in order to anticipate and calibrate their potential response in subsequent field application. In such tests, sensor cables have been directly bonded to the material under loading such as in the damage evaluation of bending beams [9, 10], efficiency evaluation of strengthening sheets for concrete structures [11], or directly stretched for performance evaluation of different cables [1] or for crack width evaluation [12]. They have also been embedded in soil for detection of cavities with collapse potential [13], in material similar to mining backfill for monitoring of rock damage [14], in rock specimens for evaluation of sliding damage [15], and in large-scale rock blocks for identification and characterization of non-uniform displacement patterns [16].

Our target application is deep underground mining where extraction can affect the stability of geological structures such as faults and dikes of much larger scale than the mine itself if these structures are close to a critical equilibrium state [17]. To better understand interactions and the farfield deformation response of the rock-mass surrounding a mine complex, several DOFSs will be grouted in boreholes surrounding an active mining block.

A critical aspect of such a monitoring exercise resides in the installation procedure details, including sensor placement approach, grout properties, and borehole size, in order to ensure that rock mass strain is accurately transferred to the sensor. Another prerequisite for sound field data interpretation is proper characterisation of the sensing system limitations in terms of measurement sensitivity, range and artefacts. These issues motivated the authors to consider a comprehensive set of experiments to understand how a sensing cable responds under various strain conditions. We report results from a sensor tested to develop knowledge on its response to various displacements, including tension and shear. The following sections will describe each part of the tests separately.

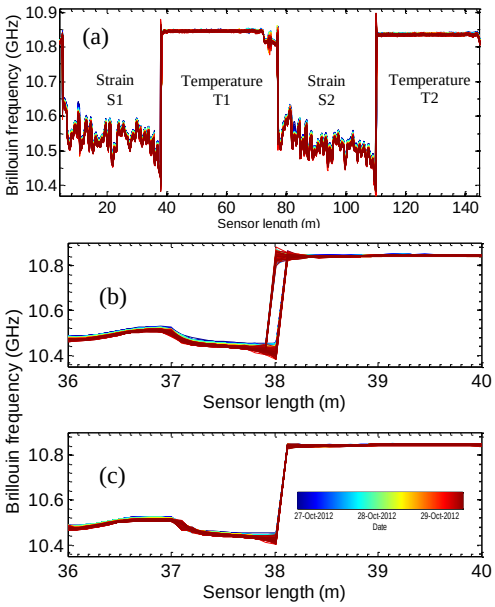

Fig. 1. a) Complete registered frequency profile, b) Shifted profile at S1-T1 location, c) Reduced shifting issue.

2. UNSTRAINED SENSOR

A series of test were first performed on unstrained DOFS in order to assess repeatability and noise level. Smartprofile™, a commercial DOFS from Smartec that includes four fibers embedded (two are dedicated for strain measurements while the other two for temperature compensation) in a polyethylene coating was used for this study, and interrogated by a BOTDA-based DiTeSt system from Omnisens. Almost 1000 measurements were obtained on a strain-free sensor in order to constrain the noise level of the sensing cable (Fig. 1.a). On raw frequency plots over the length of the sensor it was found that frequency profiles for various measurements display some problems in measurement location repeatability (Fig. 1.b). This misalignment of subsequent readings is especially clear at the large frequency step present at the strain-to-temperature sensors interface. Such location inaccuracy will particularly impact the strain interpretation since 1) the strain is derived from the difference between subsequent readings ($\Delta\nu_B$) and misalignment of measurement will induced error on the interpreted strain, and 2) the manufacturing of the Smartprofile induced

significant variations in the absolute Brioullion frequency response of the strain dedicated fibers over a short distance, thus the misalignment issue will generate significant errors.

To mitigate its effect, a simple algorithm was developed to attempt to realign locally corresponding data based on the approach shown in Fig. 2. It is based on the assumption that misalignment never exceeds one distance sampling step, which is 10 cm in our case. Three frequency changes between the initial reading (j=1) and subsequent readings (j>1) for a point i are considered and compared: $\Delta_i = \nu_{i,j}-\nu_{i,1}$, $\Delta_{i-1} = \nu_{i-1,j}-\nu_{i,1}$ and $\Delta_{i+1} = \nu_{i+1,j}-\nu_{i,1}$. The smallest value of these three differences is considered as the more reliable, and the absolute frequency readings are corrected accordingly: if Δ_i is the smallest (Fig. 2.a), $\nu_{i,j}$ is kept unchanged. If Δ_{i-1} or Δ_{i+1} are the smallest (Fig. 2.b & c) then $\nu_{i,j} = \nu_{i-1,j}$ or $\nu_{i,j} = \nu_{i+1,j}$, respectively. Fig. 1.c shows corrected raw frequencies after application of this algorithm.

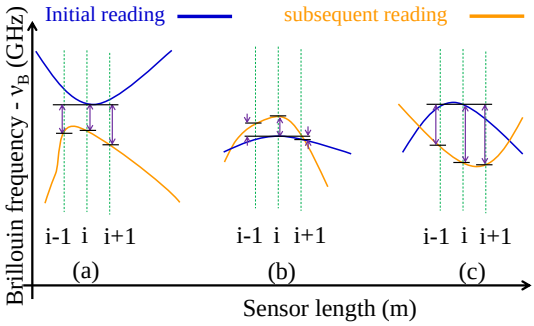

Fig. 2. Simple representation of developed algorithm for reducing the shifting issue

After such pre-filtering of the raw data, the noise in the differential readings ($\Delta\nu_B$) level is evaluated to assess realistic sensitivity of the system. This is useful for the design of subsequent lab and field scale tests in order to optimize applied load and installation locations, respectively. With a 10-cm sampling interval, Brillouin frequency is registered at 320 points along each segment of the cable (S1, T1, S2, and T2; see Fig. 1.a), resulting in a matrix of 320 × 1000. From 1000 measurements, three standard deviations (3×SD) of all 320 points were considered as a random variable and its 95% confidence interval was computed, as summarized in Table 1. Based on correlation coefficients supplied by Smartec, $\Delta\nu_B$=1 MHz equals 19.78 με and 0.8697 °C for strain and temperature, respectively. It can be seen that strain variations are constrained to less than 250 με, i.e. 0.00025, enough accuracy for detection of elastic strains remote from deep active mining (based on discrete element modeling of a rockmass containing random joints where mining occurs at depths greater than 1000 m). From Table 1, we note that the temperature measurements do not show high accuracy, implying that distributed temperature measurements based on this system are not recommended if the detection of small changes (< 3°C) is required.

Table 1. Base accuracy summary of the sensing cable

Sensors	Strain (με)			Temperature (°C)		
	S1	S2	Avg.	T1	T2	Avg.
95% CI	±107	±115	±110	±2.5	±2.8	±2.6

3. TENSIONING TEST

As the basic functionality of the Smartprofile™ is for measurement of linear deformation, it was strained using a simple setup: one end of the Smartprofile was fixed and the other end was stretched, for various lengths of strained cable from 100 cm down to 1 cm. Each length was subjected to a number of displacement increments inducing a maximum strain of 0.05%. Figure 3.a. graphs the response of each length to application of 5000 με. The system shows a clear response for lengths as short as 30 cm, almost half the spatial resolution (SR). For lengths below SR = 50 cm it is expected that the frequency response should be less than the applied one due to averaging effects, however this effect is not observed and for strained length of 40 and 30 cm the frequency shift $\Delta\nu_B$ is similar to that for the strained length of 50 cm or more.

On the other hand, no systematic $\Delta\nu_B$ is evident in Fig 3.a. for all lengths below half the SR, i.e. 25 cm. Fig. 3.b presents the magnified view of the strained section of cable for 4 lengths below SR/2. From the figure, $\Delta\nu_B$ falls within the accuracy of the unstrained cable, Table 1.

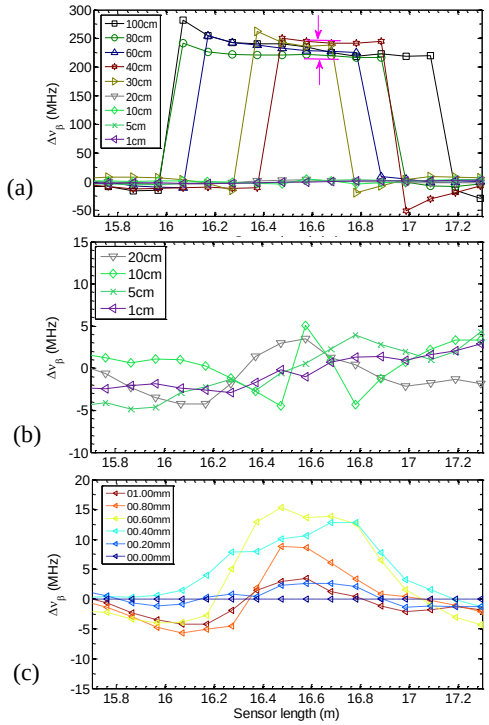

Fig. 3. a) $\Delta\nu_B$ for application of 5000 με to various lengths, b) $\Delta\nu_B$ for lengths less than SR, c) typical $\Delta\nu_B$ response applying incremental displacement to a 20 cm clamped length.

Figure 3.c shows a typical measurement for a 20 cm length of strained cable. $\Delta\nu_B$ primarily increased as the cable was stretched up to 0.6 mm, followed by a gradual decrease in $\Delta\nu_B$ for higher displacements. The reason for this response is probably the internal signal processing algorithm in the DiTeSt that ignores the high frequency peaks for lengths much smaller than the SR [18].

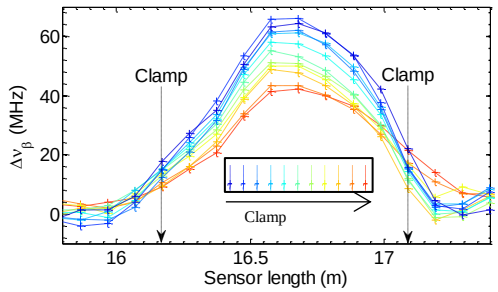

Fig. 4. Frequency response due to the effect of clamping

From Fig. 3.a, $\Delta\nu_B$ at the middle of the section (pink arrow) for different strained lengths, i.e. 30 – 100 cm, varies about 22 MHz. There are some reasons for this discrepancy. First, the initial lengths were not pretensioned in order to have a complete response from unstrained to strained state, and thus the onset of actual strain may differ slightly from one test to the next. Second, during straining, limited cable slip through the clamps may have occurred, especially at higher displacements. Third, we also identified that the clamping itself has some effect on the frequency response, as illustrated in Fig. 4. On this figure, data from a 60-cm cable length is shown for which clamps were initially tightened just enough to prevent slip, and 1 mm of stretching was applied (dark blue curve in Fig. 4). Subsequently, the clamps were gradually tightened, the tighter case being the red curve on Fig. 4. Increasing tightening reduced $\Delta\nu_B$ by about 24 MHz. In our experimental setup, clamps tightening was manually applied as consistently as possible to limit this effect.

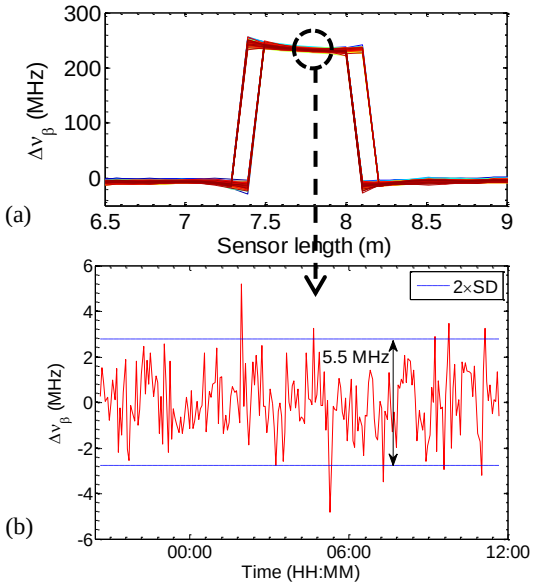

Fig. 5. a) $\Delta\nu_B$ for application of 2500με to a 60-cm clamped length over 12 hrs, b) $\Delta\nu_B$ for the mid-point of the strained length over time.

In addition to this, and also to see if the strained length shows any time-dependent behaviour, a 60-cm length was kept strained under 3 mm displacement over 15 hr, as shown in Fig. 5.a. Fig.5.b shows $\Delta\nu_B$ for the mid-point over this period after detrending caused by a 2°C temperature decrease. This figure shows that the measurements were quite repeatable during the

load time, where two standard deviations of $\Delta\nu_B$ led to only ±2.75 MHz, and no creep behavior was observed. This contrasts with results from [19] where a dead load (constant load) used for straining induced time-dependent creep of the polyethylene cable. With the current setup, i.e. fixed boundary conditions, the measurements are satisfactorily stable with time.

It is worth noting, from Fig. 4, that the frequency response presents a bell curve profile, whereas it has shown a box-car shaped profile as illustrated in most figures so far. Both shapes can be actually seen in all strained lengths. The bell curve shape is observed at lower applied strains, while as more strain is induced in the cable it gradually converts to the box-car profile, as shown in Fig.6 for a 60 cm length of strained cable. The transition occurs at about 1.5 mm of stretching for the 60 cm length.

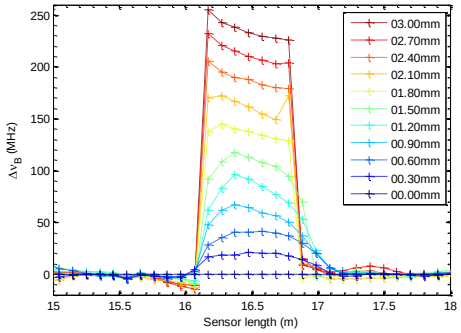

Fig. 6. Transition of $\Delta\nu_B$ profile from a bell curve shape at low strains to a boxcar mode at high strains

$\Delta\nu_B$ at the middle of strained lengths against applied microstrain for various lengths is shown in Fig. 7. The solid straight line represents the DiTeSt-recommended conversion factor. Though it seems that the line provides a good correlation for all lengths longer than SR/2, it actually overestimates the measured $\Delta\nu_B$, particularly at high strains. A new best-fit to all responsive strained lengths was obtained as C_ε = 21.52 με/MHz as graphed by the black dashed line. Also, shown as dash-dot red line, this best fit is bounded with 95% confidence interval where the upper and lower ranges are C_ε = 21. 3725 με/MHz and C_ε=21.6748 με/MHz respectively.

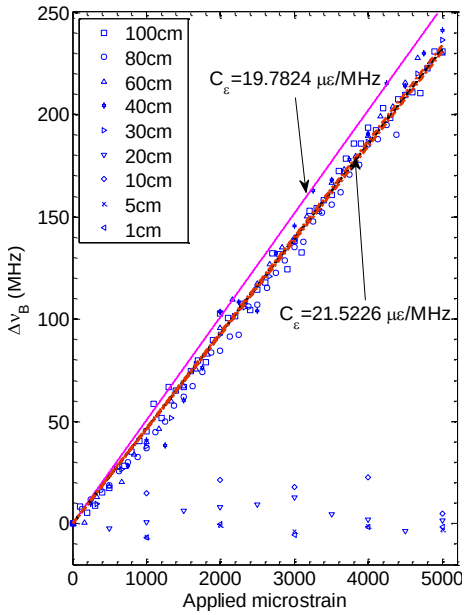

Fig. 7. $\Delta\nu_B$ for various applied strain to all lengths

4. SHEAR DISPLACEMENT

For rock mass deformation, shear mechanisms, i.e. slippage along rock joints, is a common deformation mechanism that needs to be addressed by any monitoring system dedicated to rock mass deformation. Various aspects need to be understood, including the sensitivity of the system in shear, the ability to distinguish between response in extension and response in shear, and the range of shear deformation the system can handle before measurement failure. For these reasons, a number of tests were implemented to assess the DiTeSt response when various displacements are applied normal to the longitudinal direction of different lengths of the sensing cable.

The Smartprofile™ has a rectangular cross-sectional area with radii of curvature of 5 and 1000 cm about the x and y axes (cable handling instruction from the manufacturer), respectively, as shown in Fig. 8.a. Figs. 8.c and d shows the DiTeSt frequency response to shearing for various lengths about the y axis. The cable is only able to measure linear strain, although shear displacement is applied. For the sake of comparison with tension test results, an amount of shear displacement was applied under which a linear 5000 με (~253 MHz) is induced to each length. This requires displacements almost 20

times more than the corresponding values in direct extension; e.g. for 100 cm length a 100 mm shear displacement was applied giving 5 mm in extension. It was found that all lengths down to 40 cm could register the applied strain, whereas no strain was detected below 40 cm. Compared with extension tests, shear displacement tests about the y-axis require longer lengths to detect any strain.

From Figs. 8.c and d, the $\Delta\nu_B$ profile between two clamps differs from each other for lengths above 40 cm, particularly 80 cm and 100 cm. $\Delta\nu_B$ in the S1 fibre shows an increase followed by a decrease from left to right, whereas it falls then rises in the S2 fibre. The reason for this behavior is explained in Fig. 8.b. In the test configuration, the S1 at the moving clamp side experiences tension whereas the S2 is compressed, and vice versa for a fixed clamp.

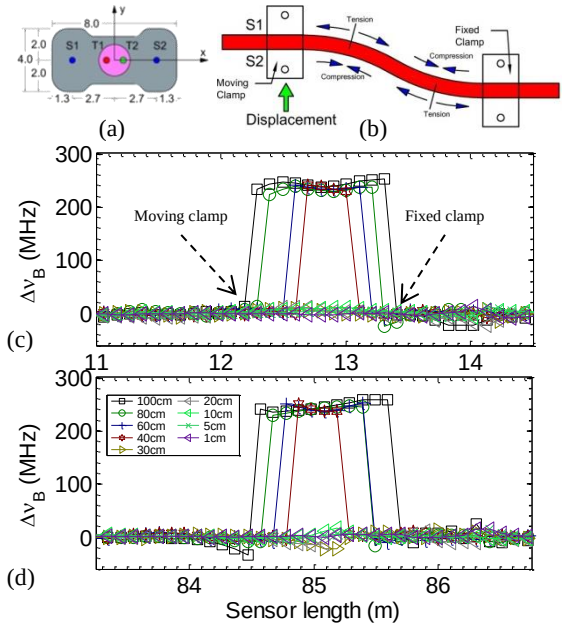

Fig. 8. a) Cross-section of Smartprofile, b) Shear displacement configuration, and $\Delta\nu_B$ for sensors c) S1, and d) S2

It should be noted from the shear test results that the $\Delta\nu_B$ rate when shear displacement increases shows a linear growing trend, while this was constant for extension tests, as shown in Fig. 9 for the mid-point of a 100-cm strained length. For example, when applying 5000 με linear strain in a shear configuration, $\Delta\nu_B$ shows 45 MHz more increase compared to the application of 50 με extension. The shear configuration can actually be seen as a trigonometry triangle, $\varepsilon_{linear} = \left(\sqrt{L_0^2 + D_s^2} - L_0\right) \Big/ L_0$, in that at higher shear displacements (D_s) more strain is registered by power of 2. The figure can actually provide a bound for a strain rate change varying from pure extension to pure shear displacement.

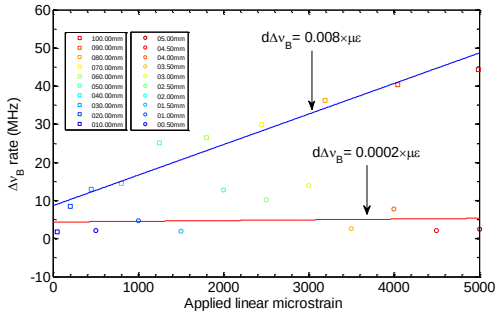

Fig. 9. $\Delta\nu_B$ rate for the extension and shear displacement application (shown as circle and square marks, respectively) to a 100-cm length

When applying shear displacement directly to the cable, a sharp kink at the location of clamps can occur, particularly at high displacements, which might affect the cable response. Directly applying shear to the cable would correspond to the non-realistic situation where the cable is directly embedded in the rock mass without using a filling material (e.g. grout) that acts as a buffer in the transmission of strain to the cable. In order to test a more realistic situation, a 100-cm length of cable embedded into a 2" dry sand filled flexible pipe was strained in a similar manner. Fig. 10 shows the frequency response along the cable length (a) and against applied shear displacement (b) for both cases. As expected, not only is much less strain registered in the case of the embedded cable, but the strain also builds up more slowly (Fig. 10.b). The standard deviations graphed in Fig. 10.b are computed from the frequency response of all points along the strained length.

5. CONCLUSIONS

Distributed fiber optic sensors are receiving more attention in mining environments not only due to their durability and insensitivity to disturbing factors such as electromagnetic fields

and noisy working areas, but also because of the attractive capability of continuously measuring deformation at many points along their lengths, over large volumes of rockmass. However, for successful technology application, confidence must be based on the actual response of such sensors under the conditions relevant for mine deformation monitoring.

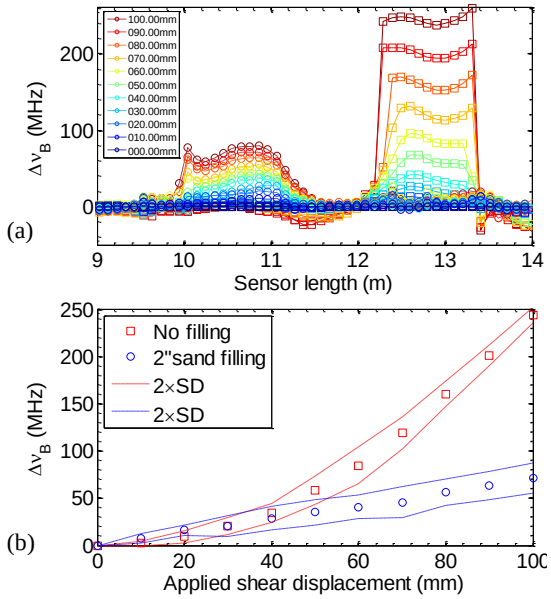

Fig. 10. $\Delta\nu_B$ response a) Along the cable length and b) Against applied shear displacement for no-filling and filled cases

A three-day free run of unstrained Smartprofile™ was done to characterise the noise level and establish what realistic sensitivity in strain and temperature should be expected. Also, a spatial shift along the length of the cable was noticed from various overlaid strain profiles, reduced using a comparative algorithm. Results showed that the system provided better performance in strain sensing with an average accuracy of 0.02% than those in temperature.

Furthermore, extensional tests on the cable while different lengths were strained showed that the strain could be accurately detected down to a length above half the claimed spatial resolution, i.e. 25 cm. Below this length, only noise was registered, highlighting a system limitation for the measurement of very localised strain. This length dictates the base requirement for future test designs and field installation considerations.

Also with these tests the frequency-strain conversion factor was re-evaluated and refined.

In the case of displacement in shear it was found that to create a pre-determined linear strain in this configuration compared with the extension set-up, a shear displacement value of 20 times more than the corresponding extension is required. This, of course, is influenced by the relative angle between the displacement direction and the cable, but on the other hand, it shows lower sensitivity of the system to shear detection. The shear detection ability became worse when embedded in flexible water pipe filled with dry sand. This implies that a better system performance in shearing would demand a more brittle, stiffer filler material in order to maximize shear transfer to the sensor cable.

ACKNOWLEDGEMENTS

This work is funded by an equipment grant from NSERC (National Sciences and Engineering Research Council of Canada), CEMI (Centre for Excellence in Mining Innovation) by the Ontario Ministry of Research and Innovation through the SUMIT (Smart Underground Monitoring and Integrated Technology) research program.

REFERENCES

[1] Iten, M. 2011. *Novel applications of distributed fiber-optic sensing in geotechnical engineering*. PhD thesis, ETH Zurich, Switzerland

[2] Johansson, S. and D. Watley. 2004. *Dam safety experiences from distributed strain measurements in five embankment dams.* Elforsk AB, Stockholm, Sweden, 2004-07:52.

[3] He, J., Z. Zhou, and O. Jinping. 2012. Optic fiber sensor-based smart bridge cable with functionality of self-sensing. *Mechanical Systems and Signal Processing* 35: 1–2, 84–94.

[4] Inaudi, D. and B. Glisic. 2006. Integration of distributed strain and temperature sensors in composite coiled tubing. In *SPIE Proceedings Vol. 6167 Smart Structures and Materials 2006: Smart Sensor Monitoring Systems and Applications 6167.1 (2006)*: 616717.

[5] Inaudi, D. and B. Glisic. 2006. Distributed fiber optic strain and temperature sensing for structural health monitoring. In *IABMAS'06 The 3rd*

Int'l Conference on Bridge Maintenance, Safety and Management, Porto, 16 – 19 July 2006.

[6] Bennett, P. J., K. Soga, H. Mohamad, C. K. Knight-Hassell, C. N. Ow, C.-S. Lim, and R. J. Mair, 2007. Monitoring Tunnel Deformation Induced by Close-Proximity Bored Tunneling Using Distributed Optical Fiber Strain Measurements. In *7th International Symposium on Field Measurements in Geomechanics, FMGM 2007*.

[7] Naruse, H., H. Uehara, T. Deguchi, K. Fujihashi, M. Onishi, R. Espinoza, C. Guzman, C. Pardo, C. Ortega, and M. Pinto. 2007. Application of a distributed fibre optic strain sensing system to monitoring changes in the state of an underground mine. *Measurement Science and Technology* 18: 10, 3202–3210.

[8] Aminossadati, S. M., N. M. Mohammed, and J. Shemshad. 2010. Distributed temperature measurements using optical fibre technology in an underground mine environment. *Tunnelling and Underground Space Technology* 25:3, 220–229.

[9] Bao, X., M. DeMerchant, A. Brown, and T. Bremner. 2001. Tensile and compressive strain measurement in the lab and field with the distributed Brillouin scattering sensor. *J. of Lightwave Technology* 19: 11, 1698–1704.

[10] Bernini, R., M. Fraldi, A. Minardo, V. Minutolo, F. Carannante, L. Nunziante, and L. Zeni. 2006. Identification of defects and strain error estimation for bending steel beams using time domain Brillouin distributed optical fiber sensors. *Smart Materials and Structures* 15: 2, 612–622.

[11] Wu, Z., B. Xu, K. Hayashi, and A. Machida. 2006. Distributed optic fiber sensing for a full-scale PC girder strengthened with prestressed PBO sheets. *Engineering Structures* 28: 7, 1049–1059.

[12] Hoepffner, R. 2008. *Distributed fiber optic strain sensing in hydraulic concrete and earth structures : measuring theory and field investigations on dams and landslides.* PhD thesis. Technische Universität München, Munich.

[13] Lanticq, V., E. Bourgeois, P. Magnien, L. Dieleman, G. Vinceslas, A. Sang, and S. Delepine-Lesoille. 2009. Soil-embedded optical fiber sensing cable interrogated by Brillouin optical time-domain reflectometry (B-OTDR) and optical frequency-domain reflectometry (OFDR) for embedded cavity detection and sinkhole warning system. *Measurement Science and Technology* 20: 3, 034018.

[14] Chai, J., S. Wei, X. Chang, and J. Liu. 2004. Monitoring deformation and damage on rock structures with distributed fiber optical sensing. *Int. J. of Rock Mechanics and Mining Sciences* 41: 3, 298–303.

[15] Tian Guo, T., W. Qing Yuan, and L. Hao Wu. 2009. Experimental research on distributed fiber sensor for sliding damage monitoring. *Optics and Lasers in Engineering* 47: 1, 156–160.

[16] Cappa, F., Y. Guglielmi, S. Gaffet, H. Lançon, and I. Lamarque. 2006. Use of in situ fiber optic sensors to characterize highly heterogeneous elastic displacement fields in fractured rocks. *Int. J. of Rock Mechanics and Mining Sciences* 43: 4, 647–654.

[17] McKinnon, S. D. 2005. Triggering of Seismicity Remote from Active Mining Excavations. *Rock Mechanics and Rock Engineering* 39: 3, 255–279.

[18] Ravet, F. , F. Briffod, B. Glisic, M. Nikles, and D. Inaudi. 2009. Submillimeter crack detection with brillouin-based fiber-optic sensors. *Sensors Journal, IEEE* 9: 11, 1391–1396.

[19] Valley, B., B. M. Madjdabadi, P. K. Kaiser, and M. B. Dusseault. 2012. Monitoring mining-induced rock mass deformation using distributed strain monitoring based on fiber optics. In *European Rock Mechanics Symposium-EUROCK 2012, Stockholm*, 28 - 30 May 2012